Published in final edited form as:
Phys Biol. 2013 February ; 10(1): 016005. doi:10.1088/1478-3975/10/1/016005.

A cortical folding model incorporating stress-dependent growth explains gyral wavelengths and stress patterns in the developing brain

PV Bayly[1,2,*], **RJ Okamoto**[2], **G. Xu**[3], **Y Shi**[2], and **LA Taber**[1,2]

[1]Department of Mechanical Engineering and Materials Science, Washington University in Saint Louis, 1 Brookings Drive, Saint Louis, Missouri 63105

[2]Department of Biomedical Engineering, Washington University in Saint Louis, 1 Brookings Drive, Saint Louis, Missouri 63105

[3]Department of Engineering and Physics, University of Central Oklahoma, 100 North University Drive, Edmond, OK 73034

Abstract

In humans and many other mammals, the cortex (the outer layer of the brain) folds during development. The mechanics of folding are not well understood; leading explanations are either incomplete or at odds with physical measurements. We propose a mathematical model in which (i) folding is driven by tangential expansion of the cortex and (ii) deeper layers grow in response to the resulting stress. In this model the wavelength of cortical folds depends predictably on the rate of cortical growth relative to the rate of stress-induced growth. We show analytically and in simulations that faster cortical expansion leads to shorter gyral wavelengths; slower cortical expansion leads to long wavelengths or even smooth (lissencephalic) surfaces. No inner or outer (skull) constraint is needed to produce folding, but initial shape and mechanical heterogeneity influence the final shape. The proposed model predicts patterns of stress in the tissue that are consistent with experimental observations.

INTRODUCTION

Cortical folding is a critical process in brain development. In the human fetus, cortical folding normally occurs between the 25th and 40th weeks of gestation. Many other mammals also have folded (gyrencephalic) brains. In the ferret, cortical folding occurs post-natally (Fig. 1), roughly between the 5th and 30th days after birth. Folding in the ferret has been thoroughly documented in seminal papers by Smart and McSherry (1, 2) and in more recent work based on MR imaging (3–5) and detailed histology (6). Abnormal folding patterns in the human brain are associated with severe mental or emotional disorders (7–11). Disturbances of cortical folding in humans include complete absence of folds (lissencephaly), folds that are abundant but small and shallow (polymicrogyria), and folds that are fewer and coarser (pachygyria). Despite decades of intense study (12–15) and speculation, the mechanical basis of folding remains controversial.

Van Essen (16) has proposed that *axonal tension* produces folding by drawing sides of gyri (outward folds) together. This hypothesis is attractive because it is consistent with efficient wiring – axons that connect related areas will draw them together, decreasing the total length

Corresponding author: Philip V. Bayly, PhD, Mechanical Engineering and Materials Science, 1 Brookings Drive, Box 1185, Saint Louis, Missouri 63130, TEL: 314-935-6081, baylyp@seas.wustl.edu.

of axonal connections. Heidemann and co-authors (17–19) have shown that axons in vitro maintain tension. Dissection experiments (20, 21) have confirmed that white matter in mammalian brains is under tension, including the white matter in the adult mouse brain (20) and in both mature and developing ferret brains (21). However the hypothesis that the walls of gyri are drawn together by axonal tension is not consistent with observed patterns of stress in the ferret brain, which reflect tension along, not across, gyri (21) (Fig. 1).

Other authors (22, 23) have pointed to *differential growth*, in which outer layers grow tangentially at faster rates than inner layers of the brain, as the driving mechanism of cortical folding. Richman and coauthors (23) proposed a model for the formation of cortical folds based on buckling of elastic surface layers on an elastic foundation. In this scenario, tangential growth of the outermost layer produces compressive stress that leads to buckling of this layer, modulated by the stiffness of the foundation. In terms of developmental neuroanatomy (see (24)) the outer layers in this model comprise the cortical plate, and the foundation, or core, captures the aggregate mechanical behavior of subplate, intermediate zone, subventricular zone, ventricular zone, and all deeper internal brain structures. In the Richman model (23), increasing the material stiffness, or elastic modulus, of the foundation leads to shorter wavelengths of the buckled layer (cortex). However, this model and other elastic buckling models (22) rely on a large mismatch in the elastic moduli of the outer layer (stiffer) and core (softer) to produce buckling patterns that approximate observed folds. In fact, the elastic modulus of the outer layer of cortex is not significantly different than that of inner regions of the brain (25–27).

The question we address is: What mechanism can produce folded surfaces with wavelengths consistent with those observed in nature, and stress patterns consistent with those seen in dissection experiments, without requiring a difference in elastic modulus between layers? We propose a model of folding in which tangential growth of the cortex drives the folding process. Instead of a purely elastic foundation (22, 23), or a hard constraint (28), the core is allowed to grow in response to the resulting stresses. Axons, which are the major functional component of white matter, are known to grow in response to imposed tension (19). The proposed model produces surface folding in which the wavelength depends on the rate of cortical growth relative to the rate constant of the stress-growth relationship in the core. Patterns analogous to polymicrogyria and pachygyria can be obtained by adjusting this ratio. The pattern of folding-induced stress is consistent with observations of stress in the developing ferret brain, in which tension exists along the radial axis of gyri.

MATHEMATICAL MODEL AND SIMULATION

Our mathematical model of cortical folding uses the theory of volumetric growth developed by Rodriguez et al. (29) and applied in many studies since (30–33). Using standard continuum mechanics terminology, we designate the location of a material element in the reference configuration as $\boldsymbol{X}$ and the corresponding location of the same element in the deformed configuration as $\boldsymbol{x}$. The deformation gradient tensor is $\boldsymbol{F}=\frac{\partial \boldsymbol{x}}{\partial \boldsymbol{X}}$. According to the theory of Rodriguez et al. (29), $\boldsymbol{F}$ is expressed as the product of a growth tensor, $\boldsymbol{G}$, and an elastic tensor, $\boldsymbol{F}^*$:

$$\boldsymbol{F}=\boldsymbol{F}^{*}\cdot\boldsymbol{G}. \quad (1)$$

Numerous material models have been suggested to describe the mechanical behavior of brain tissue. Recent studies have proposed isotropic, hyperelastic or hyper-viscoelastic models for grey matter (26, 34, 35), and anisotropic, hyperelastic or hyper-viscoelastic models for white matter (36, 37). At relatively short time scales (shorter than those

associated with growth) cortical brain tissue may be roughly approximated as an isotropic, hyperelastic material (26), so the Cauchy stress tensor, $\boldsymbol{\sigma}$, depends directly on the elastic deformation according to the constitutive relationship

$$\sigma = J^{*-1}\boldsymbol{F}^{*}\cdot\frac{\partial W}{\partial \boldsymbol{F}^{*T}}. \quad (2)$$

Here $\boldsymbol{W}$ is the strain energy density function for the material and J^{*} = det $\boldsymbol{F}^{*}$ is the volume ratio of the elastic deformation. A standard neo-Hookean material model (38) is used here:

$$W=\frac{\mu}{2}(I_1^{*}J^{*-2/3}-3)+\frac{\kappa}{2}(J^{*}-1)^2. \quad (3)$$

The strain energy depends on J^{*} and on the first invariant (trace) of the elastic right Cauchy-Green strain tensor, $I_1^{*}=tr\,\boldsymbol{C}^{*}$, where $\boldsymbol{C}^{*}=\boldsymbol{F}^{*\boldsymbol{T}}\cdot\boldsymbol{F}^{*}$. The shear modulus, μ, and the bulk modulus κ, , are the parameters of the hyperelastic model. Typically tissue is assumed to be nearly incompressible: $\kappa \gg \mu$.

Radial and tangential normal growth are included in the current model. Simulations are performed in (i) a two-dimensional (2D) rectangular domain in plane strain, approximating a section of tissue near the cortical surface, (ii) a 2D semi-elliptical domain in plain strain (approximating a section of an elliptical cylinder), and (iii) an axisymmetric ellipsoidal domain. In the 2D rectangular and elliptical domains, growth is modeled using:

$$\boldsymbol{G}=G_r\boldsymbol{e}_r\boldsymbol{e}_r+G_t\boldsymbol{e}_t\boldsymbol{e}_t, \quad (4)$$

where $\boldsymbol{e}_i\,\boldsymbol{e}_j$ denotes the tensor product of unit vectors $\boldsymbol{e}_i$ and $\boldsymbol{e}_j$. In the rectangular domain the "radial" direction (normal to the free surface) is vertical and the tangential direction is horizontal.

In the axisymmetric ellipsoid, growth is modeled using:

$$\boldsymbol{G}=G_R\boldsymbol{e}_R\boldsymbol{e}_R+G_t\boldsymbol{e}_t\boldsymbol{e}_t+G_t\boldsymbol{e}_\varphi\boldsymbol{e}_\varphi, \quad (5)$$

where azimuthal (φ) growth is assumed equal to the in-plane tangential growth. In Eqs. 4–5 the radial and tangential directions are defined in a standard elliptical or ellipsoidal coordinate system. In both models, the thin upper layer (the cortex) grows tangentially only at a constant rate, G_0. In deeper layers (the foundation, or core) growth ensues in response to stress.

$$\text{Cortex:}\quad G_t=1+G_0t,\qquad G_r=1. \quad (6)$$

$$\text{Core:}\quad \frac{\partial G_r}{\partial t}=a(\sigma_{rr}-\sigma_{r0})G_r,\qquad \frac{\partial G_t}{\partial t}=a(\sigma_{tt}-\sigma_{t0})G_t. \quad (7)$$

The parameters σ_{t0} and σ_{t0} are "target" stresses for the core; growth will continue until these stress values are reached. The parameter a (units: 1/Pa-s or 1/Pa-hr) determines how rapidly variations in growth occur in response to variations in radial or tangential normal stress (σ_{rr} or σ_{tt}). For simplicity we assume a is the same in both directions. A very rough estimate of $a\sim3\times10^{-3}$/Pa-hr may be obtained for white matter from the experiments of Chada et al. (19) who determined neurite elongation rates of 200 μm/hr under tension of 2 pN (200 μdyne).

The stiffness of the material in the core will also affect how quickly it responds to cortical growth. For an incompressible material undergoing small, uniaxial, plane-strain deformations, the stress-strain relationship is $\sigma = 4\mu_f \varepsilon$, where ε is the strain and μ_f is the shear modulus of the core (the subscript f denoting "foundation" is used to distinguish core from cortex). Defining dimensionless stress $\bar{\sigma} = \sigma/4\mu_f$, we can rewrite Eqs. 7 as

$$\frac{\partial G_r}{\partial t} = 4\mu_f a(\bar{\sigma}_{rr} - \bar{\sigma}_{r0})G_r \qquad \frac{\partial G_t}{\partial t} = 4\mu_f a(\bar{\sigma}_{tt} - \bar{\sigma}_{t0})G_t \quad (8)$$

It is apparent that the rate constant governing the response of the core to imposed deformation is $R_f = 4a\mu_f$ (units: 1/s). Fully dimensionless versions of Eqs. 6–7 can be obtained using $\tau = G_0 t$.

$$\text{Cortex:} \quad G_t = 1 + \tau \qquad G_r = 1 \quad (9)$$

$$\text{Core:} \quad \frac{\partial G_r}{\partial \tau} = \frac{R_f}{G_0}(\bar{\sigma}_{rr} - \bar{\sigma}_{r0})G_r \qquad \frac{\partial G_t}{\partial \tau} = \frac{R_f}{G_0}(\bar{\sigma}_{tt} - \bar{\sigma}_{t0})G_t \quad (10)$$

Finite element simulations of the rectangular, elliptical and ellipsoidal models were performed using COMSOL Multiphysics software (V.4.3, COMSOL Inc., Burlington, MA). Routine simulations in the rectangular domain were performed with 2412 rectangular elements; in the 2D ellipse and axisymmetric ellipsoid the domain was discretized into 2498 triangular elements. Quasi-static, time-dependent simulations were performed with the COMSOL backward differentiation formula (BDF) algorithm with maximum absolute error tolerance $< 10^{-7}$ and relative error tolerance $< 10^{-6}$. Since the locations of spatial instabilities are extremely sensitive to imperfections in numerical models, small imperfections were deliberately introduced by simulating low levels of radial growth in the core in the early stages of the simulation. Folding was typically initiated by these imperfections but the folding pattern was not solely determined by the imperfection field. The robustness of solutions with respect to discretization (mesh size and time step) was confirmed by reproducing results with finer mesh resolution and smaller error tolerances.

Analytical prediction of critical stress and wavelength

The time scale of folding is long enough for the brain to grow significantly in response to stress; such growth in the core would lead to relaxation of the stresses induced by cortical growth. The behavior of the core thus approximates the response of a viscoelastic material, specifically a Maxwell fluid. Biot (39) developed a theory for the folding instability of a thin, laterally compressed, viscoelastic plate embedded in a viscoelastic continuum. The theory of Biot (39) may be extended to the situation in which compressive stress is due to tangential growth of a thin elastic plate with thickness h (the cortex) and the embedding medium grows according to the laws in Eq. 7. According to this analysis (shown in the Appendix) we predict that the wavelength of folds, λ, will depend on the ratio $\Gamma_G = G_0/R_f$, the ratio of cortical growth to the rate constant of stress induced growth, and $\beta = \mu/\mu_f$, the ratio of the short-term elastic moduli of cortex (μ) and core (μ_f). Specifically we predict that,

$$\frac{\lambda}{h} = 2\pi\left(\frac{\beta(\Gamma+1)}{3\Gamma}\right)^{1/3}, \quad (11)$$

where Γ is the largest positive real root of the polynomial equation,

$$\Gamma^5 - \frac{64}{9}\beta^2\Gamma_G{}^3(\Gamma^2+2\Gamma+1)=0. \quad (12)$$

In this analysis, existence of at least one positive real root of Eq. 12 indicates that folding will occur at the given values of growth rate and material parameters. In the present study, for each parameter combination only one real root of Eq. 12 was found and thus only one wavelength is predicted.

RESULTS

Simulations

Growth was simulated using the mathematical description given by Eqs. (1–10). The material models for both cortex and subcortical foundation were hyperelastic (neo-Hookean). In the cortex, the constant growth rate in the direction tangent to the surface was specified to be G_0, and there was no growth in the radial direction (normal to the cortical surface). In the foundation, tangential and radial growth were stimulated by corresponding stress components, as described by the first-order relationships in Eqs. 7.

In all simulations the modulus ratio β between cortex and core was set to 1 unless noted otherwise. Using the rough estimates a~3×10^{-3}/Pa-hr and shear modulus μ~300 Pa leads to an estimate of the growth rate constant R_f~1/hr for axons in vitro, which is probably an upper bound for heterogeneous tissue in vivo. In the ferret the surface area doubles roughly every four days during the period of folding; this corresponds to a circumferential growth rate G_0~0.01/hr – 0.04/hr. Results are described at specific values of scaled time: $\tau = G_0 t$.

Effect of growth rate on folding wavelength

Simulations of a growing cortical plate of thickness $h = 0.05$ on a rectangular foundation of length $L = 2$ and $H = 1$ were performed while varying the ratio (Γ_G) of the cortical growth rate, G_0, to the rate constant, R_f, governing the stress-induced growth of subcortical layers. To ensure that folding was initiated in the center of the domain, a small initial imperfection was introduced by specifying small, positive radial growth in a narrow central band of width δ in the core, using the following modified version of Eq. 10_1. The final pattern was insensitive to δ for $\delta \leq 0.1$, so $\delta = 0.05$ was used.

$$\frac{\partial G_r}{\partial \tau} = \frac{1}{\Gamma_G}(\overline{\sigma}_{rr} - \overline{\sigma}_{r0})G_r + F(x,\tau); \quad F(x,\tau) = \begin{cases} \frac{1}{\Gamma_G}\tau, \text{ for } |x|<\delta \text{ and } \tau<0.01. \\ 0, \text{otherwise} \end{cases} \quad (13)$$

The results of these simulations are shown in Fig. 2, which depicts the growth ratios G_r and G_t, and the growth-induced stresses σ_{rr}, and σ_{tt} for $\Gamma_G = G_0/R_f = 2.5\times10^{-2}$, 2.5×10^{-3}, 2.5×10^{-4}, and 2.5×10^{-5}. The wavelength clearly *increases* as the cortical growth ratio Γ_G *decreases*. Also, as expected, the wavelength in simulations scales with the thickness of the cortical layer (Fig. 3). The wavelengths observed in simulations are close to the wavelengths predicted using Eqs. 11–12 (Fig. 4) and clearly follow the analytically-predicted trend.

Patterns of differential growth and stress

Some features of the patterns of growth-induced stress observed in Fig. 2 are consistent with previous experimental observations of tissue stress (21) summarized in Fig. 1. Radial tension is evident within the core of gyri, and tangential tension in the core is highest below

fundi. However, in the model tangential tension is also seen within the core of gyri. We hypothesized that the tangential tension in the outermost layer of the core arises because in the basic model growth is imposed only in the cortex, which is modeled as a completely separate outer layer. Tangential growth thus occurs in the outer core only in response to stress, leading to a sharp discontinuity in tangential growth at the interface. In reality, there is a fairly smooth gradient in tangential growth (6) from the outer cortical layer. We model this by having the target tangential stress in the outer core track the imposed compressive tangential stress in the cortex and decay smoothly and rapidly with distance from the interface ($r = H$).

$$\sigma_{t0} = -4\mu\tau\, e^{20(r-H)} \quad (14)$$

With this modification the dependence of wavelength on cortical growth rate is maintained, but the tangential stress within gyri becomes compressive (Fig. 5), consistent with observations (Fig. 1, (21)).

Effects of shape, initial conditions, and cortical growth rate

To consider the effects of the geometry of the entire brain while retaining computational simplicity, we simulated cortical growth in (i) a cylinder with elliptical cross section, and (ii) an axisymmetric ellipsoid. A 2D elliptical region undergoing plane strain was used to model the cylindrical case. In both cases the major and minor semi-axes of the elliptical cross-section were $A = 1.2$ and $B = 1.0$ and the thickness of the cortical layer was $h = 0.05$. In the 2D ellipse, the radial coordinate $r = \sqrt{\frac{x^2}{A^2} + \frac{y^2}{B^2}}$ and in the axisymmetric ellipsoid $R = \sqrt{\frac{z^2}{A^2} + \frac{r^2}{B^2}}$.

As in the rectangular domain, folding was facilitated by specifying initial radial growth in the core, either in a small band (as in Eq. 13, but for $|\theta| < \delta$), or as a harmonic or random field (Eq. 15, below).

$$\frac{\partial G_r}{\partial \tau} = \frac{1}{\Gamma_G}(\overline{\sigma}_{rr} - \overline{\sigma}_{r0})G_r + F(r,\theta,\tau) \qquad \begin{cases} F(r,\theta,\tau) = F_0\tau\cos k\theta;\ \tau<0.1 \text{ or} \\ F(r,\theta,\tau) = F_0\tau\,\text{random}(r,\theta);\ \tau<0.1 \end{cases} \quad (15)$$

Here F_0 defines the magnitude of the initial shape perturbation. Both the elliptical geometry and the initial conditions influenced folding patterns. At similar parameter values, longer wavelengths were seen in the ellipse and ellipsoid than in the rectangular domain (Fig. 6), but the general dependence of wavelength on cortical growth rate remained. Converged folded solutions were found in a smaller range of Γ_G; at small Γ_G the growth of the core prevented critical compressive stress from being reached and at large Γ_G the core seemed too stiff to allow significant deflection.

Cortical growth rate affects wavelength in the 2D elliptical domain and axisymmetric ellipsoid, as in the rectangular domain. In the ellipse and ellipsoid, simulations typically show that the instability occurs later, allowing the domain to expand significantly (Fig. 6). We observe that, as in the rectangular domain, the wavelength increases as Γ_G decreases; however the number of waves per angular increment remains fairly constant. For a given value of Γ_G the wavelength $\lambda_{rectangle} < \lambda_{ellipse} < \lambda_{ellipsoid}$, which is consistent with the structural stiffening effect of curvature.

Folding patterns exhibited by the elliptical cylinder in response to cortical growth (Eqs. 1–10, 15) are shown in Fig. 7 for three sets of harmonic and random initial conditions. Note that the final shape appears to be affected by even slight variations in the initial shape. However, fine-grained random initial conditions lead to a relatively coarse folding pattern, confirming that material and structural properties play an important role in determining wavelength.

Heterogeneous initial conditions do not completely determine the final shape; the cortical growth rate remains important. In Fig. 9 (Row 1) we see that the initial field with spatial frequency four time less than the initial field in Fig. 8 leads to a final field with the same short wavelength; the growth rate ($\Gamma_G = 0.50$) appears to be the critical factor. For the identical initial conditions but slower cortical growth ($\Gamma_G = 0.20$) almost no folding occurs (Fig. 9, Row 2). Amplifying the initial radial growth of the core to the point that initial shape is clearly deformed (Fig. 10) leads to hybrid shapes with both wavelengths represented. One interpretation of Fig. 10 is that the initial shape determines the locations of primary folds, and the cortical growth rate mediates the formation of secondary gyri and sulci.

Effects of spatial variations in tangential cortical growth

The consistent locations of primary cortical folds might, alternatively, be due to intrinsic spatial variations in cortical growth rate. The qualitative effects of such variations can be captured by replacing the dimensionless equation for uniform cortical growth (Eq. 9_1) with

$$\text{Cortex:} \quad G_t = 1 + \tau(1 + 0.1\cos 8\theta) \quad (16)$$

No initial imperfection or growth in the core was imposed. These spatial variations in tangential growth appear to drive the ellipsoid toward a final shape with the same number of lobes as the growth pattern, with gyri at regions of greatest expansion and sulci at regions of least expansion (Fig. 11). However, short wavelength instabilities may be superimposed on this pattern (Fig. 11, row 1) if the cortical growth rate is high enough. If intrinsic variations in tangential growth rate do indeed lead to consistently located primary folds, growth-induced instability remains the likely cause of secondary gyri.

DISCUSSION

Evaluation of cortical folding hypotheses

The analysis and simulations presented here support the hypothesis that differential tangential growth of the cortex, rather than axonal tension, drives the folding process. The current model is distinct from previous models of differential growth that treat the brain as a layered elastic body (22, 23). The essential feature of the current model is that deeper layers grow in response to stresses developed by cortical expansion. While axonal tension-driven models (16) and models in which the cortex is pushed outward by growth (40) may produce realistic shapes similar to the folded brain, geometric similarity is not strong evidence of the underlying hypotheses. The stress states predicted by such models are not consistent with experimental observations described in (21). The predictions of the current model, using reasonable estimates of parameters from experimental studies (5, 19) are consistent with both observed folding patterns and observed stress distributions (21).

We previously introduced a model of cortical folding (21) which also included stress-dependent growth in deeper layers. The prior model included more layers with different specified growth rates in each layer, but relied on limiting cortical growth to a specific region to induce a single local fold in that region. In contrast, the current model relies on

instability to produce folding patterns in which wavelength depends on the relative rates of growth.

While growth-induced instability is suggested to underlie the more random, shorter-wavelength secondary folds, two candidate mechanisms are identified for the formation of primary gyri. (i) Heterogeneous radial growth before the period of folding may set up small variations in initial conditions (shape, stiffness, or stress) that are amplified by tangential expansion of the cortex. We note that axonal tension, while not actively producing folds, may be an important feature of such an initial state. (ii) Tangential cortical expansion itself may be heterogeneous, as in (21). Current experimental data do not disprove either of these possibilities. It is clear that the shape of the brain before folding is not perfectly smooth (1–4); we have also observed that on a coarse scale, cortical expansion is nonuniform (5). More precise and better resolved measurements are needed to determine the relative importance of these mechanisms in determining gyral location.

Some investigators have made important predictions regarding cortical folding without directly addressing the causal mechanism. Todd (41) suggested that initial curvature determines the folding pattern, with sulci evolving from lines of minimal curvature. This is consistent with the effects of initial shape exhibited by the current model. Prothero and Sundstren (42) use scaling arguments to arrive at plausible shapes, but do not address mechanical forces.

Elastic and hyperelastic models of wrinkling and creasing of soft tissue

A number of recent theoretical studies (28, 43–47) have demonstrated that instabilities of surfaces or layers in elastic and hyperelastic materials arise in response to compression or constrained growth. These models of soft hyperelastic materials can produce folds or creases like those seen in the brain. The current model shares many of the features of these elastic models, but emphasizes the role of stress-induced growth, rather than elastic deformation, in predicting the geometry, wavelengths and stress fields associated with folding. The current model not only produces reasonable predictions of folding patterns and stress distributions, but more accurately reflects the behavior of the living brain tissue on these time scales.

Limitations

Both analytical predictions of gyral wavelength and numerical simulations were performed. There is a consistent discrepancy of approximately 25% between the wavelengths observed in simulations and the predictions of the stability analysis (Fig. 4, Eqs. 11–12, and the Appendix). The analysis is based on the simplest theoretical model developed by Biot (39) for folding of a viscoelastic layer embedded in a viscoelastic medium. In this model, the adhesion (tangential traction) between core and cortex was neglected, and the dimensions of the foundation (L,H) were assumed to be infinite. Furthermore, the replacement of the operator R by the inverse of the time to reach critical stress, $R=\frac{1}{T_P}=4\mu G_0/\sigma_P$, is an ad hoc assumption that is physically reasonable but not mathematically precise. Despite the relatively small quantitative discrepancy between Eqs. 11–12 and simulations, the correct prediction of the inverse relationship between growth rate and wavelength is a valuable insight from the analysis.

Although cortical folding is truly a 3D process, simulations were performed in 2D, assuming either plane strain conditions or axisymmetric deformation. While 2D mechanical models have proven useful for understanding 3D behavior, it is clear that ultimately 3D models will be required to study characteristic folding patterns. Similarly, the boundary conditions in the current model, particularly the assumption of zero force on the cortical surface, are

idealized. Our results show that boundary forces are not necessary to produce folding, but do not exclude the possibility that boundary conditions play an important role. Also, other mechanisms (such as axonal connectivity) could modulate shapes produced by differential cortical expansion and stress-induced growth.

Future work

The current study is focused on the generic mechanisms that govern the initial formation and wavelengths of gyri. Further numerical studies should explore the large-deformation, "post-buckled" behavior of these models. Such studies will need to exploit more advanced simulation techniques to achieve convergence and accuracy under these conditions. The domains of the current simulations are extremely simple; the extension of modeling and simulation to the full 3D case with realistic initial shapes (as in (43)) is clearly warranted.

Conclusions

A model of cortical folding based on differential growth, in which the stiffnesses of the cortex and interior regions of the brain are similar, can explain both (i) variations in wavelength of folds and (ii) the stress fields observed in the developing brain. Cortical growth rate, relative to how quickly the core grows in response to stress, affects the wavelength of cortical folds; more rapid cortical expansion generally leads to shorter wavelengths. Wavelengths also scale directly with cortical thickness. Finally, the initial shape before tangential cortical expansion, and spatial variations in tangential expansion itself, also affect the final shape.

Acknowledgments

Funding from NIH grant R01 NS070918 (Taber), R21 EB005834 (Bayly) and NSF grant DMS0540701 (Taber) is gratefully acknowledged. C.D. Kroenke provided invaluable suggestions.

References

1. Smart IH, McSherry GM. Gyrus formation in the cerebral cortex of the ferret. II. Description of the internal histological changes. J Anat. 1986 Aug.147:27–43. [PubMed: 3693076]
2. Smart IH, McSherry GM. Gyrus formation in the cerebral cortex in the ferret. I. Description of the external changes. J Anat. 1986 Jun.146:141–52. [PubMed: 3693054]
3. Neal J, Takahashi M, Silva M, Tiao G, Walsh CA, Sheen VL. Insights into the gyrification of developing ferret brain by magnetic resonance imaging. J Anat. 2007 Jan; 210(1):66–77. [PubMed: 17229284]
4. Barnette AR, Neil JJ, Kroenke CD, Griffith JL, Epstein AA, Bayly PV, et al. Characterization of brain development in the ferret via MRI. Pediatr Res. 2009 Jul; 66(1):80–4. [PubMed: 19287340]
5. Knutsen AK, Kroenke CD, Chang YV, Taber LA, Bayly PV. Spatial and Temporal Variations of Cortical Growth during Gyrogenesis in the Developing Ferret Brain. Cereb Cortex. 2012 Feb 23.
6. Reillo I, de Juan Romero C, Garcia-Cabezas MA, Borrell V. A role for intermediate radial glia in the tangential expansion of the mammalian cerebral cortex. Cereb Cortex. 2011 Jul; 21(7):1674–94. [PubMed: 21127018]
7. Hardan AY, Jou RJ, Keshavan MS, Varma R, Minshew NJ. Increased frontal cortical folding in autism: a preliminary MRI study. Psychiatry Res. 2004 Sep 15; 131(3):263–8. [PubMed: 15465295]
8. Nordahl CW, Dierker D, Mostafavi I, Schumann CM, Rivera SM, Amaral DG, et al. Cortical folding abnormalities in autism revealed by surface-based morphometry. J Neurosci. 2007 Oct 24; 27(43):11725–35. [PubMed: 17959814]
9. Cachia A, Paillere-Martinot ML, Galinowski A, Januel D, de Beaurepaire R, Bellivier F, et al. Cortical folding abnormalities in schizophrenia patients with resistant auditory hallucinations. Neuroimage. 2008 Feb 1; 39(3):927–35. [PubMed: 17988891]

10. Sallet PC, Elkis H, Alves TM, Oliveira JR, Sassi E, Campi de Castro C, et al. Reduced cortical folding in schizophrenia: an MRI morphometric study. Am J Psychiatry. 2003 Sep; 160(9):1606–13. [PubMed: 12944334]
11. Pavone L, Rizzo R, Dobyns WB. Clinical manifestations and evaluation of isolated lissencephaly. Childs Nerv Syst. 1993 Nov; 9(7):387–90. [PubMed: 8306352]
12. Le Gros Clark, WE. Deformation patterns in the cerebral cortex. In: Le Gros Clark, WE.; Medawar, PB., editors. Essays on Growth and Form. London: Oxford University Press; 1945. p. 1-22.
13. Barron DH. An experimental analysis of some factors involved in the development of the fissure pattern of the cerebral cortex. Journal of Experimental Zoology. 1950; 113:553–81.
14. Hofman MA. On the Evolution and Geometry of the Brain in Mammals. Prog Neurobiol. 1989; 32(2):137–58. [PubMed: 2645619]
15. Welker, W. Why does the cortex fissure and fold: A review of determinants of gyri and sulci. In: Jones, EG.; Peters, A., editors. Cerebral Cortex: Comparative Structure and Evolution of Cerebral Cortex. New York: Plenum Press; 1990. p. 3-136.
16. Van Essen DC. A tension-based theory of morphogenesis and compact wiring in the central nervous system. Nature. 1997 Jan 23; 385(6614):313–8. [PubMed: 9002514]
17. Heidemann SR, Buxbaum RE. Tension as a regulator and integrator of axonal growth. Cell Motil Cytoskeleton. 1990; 17(1):6–10. [PubMed: 2225090]
18. Heidemann SR, Buxbaum RE. Mechanical tension as a regulator of axonal development. Neurotoxicology. 1994 Spring;15(1):95–107. [PubMed: 8090366]
19. Chada S, Lamoureux P, Buxbaum RE, Heidemann SR. Cytomechanics of neurite outgrowth from chick brain neurons. J Cell Sci. 1997 May; 110(Pt 10):1179–86. [PubMed: 9191042]
20. Xu G, Bayly PV, Taber LA. Residual stress in the adult mouse brain. Biomech Model Mechanobiol. 2009 Aug; 8(4):253–62. [PubMed: 18651186]
21. Xu G, Knutsen AK, Dikranian K, Kroenke CD, Bayly PV, Taber LA. Axons pull on the brain, but tension does not drive cortical folding. J Biomech Eng. 2010 Jul.132(7):071013. [PubMed: 20590291]
22. Raghavan R, Lawton W, Ranjan SR, Viswanathan RR. A continuum mechanics-based model for cortical growth. Journal of Theoretical Biology. 1997 Jul 21; 187(2):285–96.
23. Richman DP, Stewart RM, Hutchinson JW, Caviness VS. Mechanical Model of Brain Convolutional Development. Science. 1975; 189(4196):18–21. [PubMed: 1135626]
24. Bystron I, Blakemore C, Rakic P. Development of the human cerebral cortex: Boulder Committee revisited. Nat Rev Neurosci. 2008 Feb; 9(2):110–22. [PubMed: 18209730]
25. Chatelin S, Constantinesco A, Willinger R. Fifty years of brain tissue mechanical testing: from in vitro to in vivo investigations. Biorheology. 2010; 47(5–6):255–76. [PubMed: 21403381]
26. Prange MT, Margulies SS. Regional, directional, and age-dependent properties of the brain undergoing large deformation. J Biomech Eng. 2002 Apr; 124(2):244–52. [PubMed: 12002135]
27. van Dommelen JA, van der Sande TP, Hrapko M, Peters GW. Mechanical properties of brain tissue by indentation: interregional variation. J Mech Behav Biomed Mater. 2010 Feb; 3(2):158–66. [PubMed: 20129415]
28. Jin L, Cai S, Suo Z. Creases in soft tissue generated by growth. EPL. 2011; 95:64002.
29. Rodriguez EK, Hoger A, McCulloch AD. Stress-dependent finite growth in soft elastic tissues. J Biomech. 1994 Apr; 27(4):455–67. [PubMed: 8188726]
30. Lin IE, Taber LA. A model for stress-induced growth in the developing heart. J Biomech Eng. 1995 Aug; 117(3):343–9. [PubMed: 8618388]
31. Taber LA, Chabert S. Theoretical and experimental study of growth and remodeling in the developing heart. Biomech Model Mechanobiol. 2002 Jun; 1(1):29–43. [PubMed: 14586705]
32. Alford PW, Taber LA. Computational study of growth and remodelling in the aortic arch. Comput Methods Biomech Biomed Engin. 2008 Oct; 11(5):525–38. [PubMed: 18792831]
33. Tsamis A, Cheng A, Nguyen TC, Langer F, Miller DC, Kuhl E. Kinematics of cardiac growth: in vivo characterization of growth tensors and strains. J Mech Behav Biomed Mater. 2012 Apr. 8:165–77. [PubMed: 22402163]

34. Miller K, Chinzei K. Mechanical properties of brain tissue in tension. J Biomech. 2002 Apr; 35(4): 483–90. [PubMed: 11934417]
35. Miller K, Chinzei K. Constitutive modelling of brain tissue: experiment and theory. J Biomech. 1997 Nov-Dec;30(11–12):1115–21. [PubMed: 9456379]
36. Ning X, Zhu Q, Lanir Y, Margulies SS. A transversely isotropic viscoelastic constitutive equation for brainstem undergoing finite deformation. J Biomech Eng. 2006 Dec; 128(6):925–33. [PubMed: 17154695]
37. Prange MT, Meaney DF, Margulies SS. Defining brain mechanical properties: effects of region, direction, and species. Stapp Car Crash J. 2000 Nov.44:205–13. [PubMed: 17458728]
38. Holzapfel, GA. Nonlinear solid mechanics : a continuum approach for engineering. Chichester; New York: Wiley; 2000.
39. Biot MA. Folding instability of a layered viscoelastic medium under compression. Proceedings of the Royal Society of London - Series A. 1957; 242:444–54.
40. Mota B, Herculano-Houzel S. How the cortex gets its folds: an inside-out, connectivity-driven model for the scaling of Mammalian cortical folding. Front Neuroanat. 2012; 6:3. [PubMed: 22347170]
41. Todd PH. A Geometric Model for the Cortical Folding Pattern of Simple Folded Brains. Journal of Theoretical Biology. 1982; 97(3):529–38. [PubMed: 6813602]
42. Prothero JW, Sundsten JW. Folding of the Cerebral-Cortex in Mammals - a Scaling Model. Brain Behav Evolut. 1984; 24(2–3):152–67.
43. Nie J, Guo L, Li G, Faraco C, Stephen Miller L, Liu T. A computational model of cerebral cortex folding. J Theor Biol. 2010 May 21; 264(2):467–78. [PubMed: 20167224]
44. Kucken M, Newell AC. Fingerprint formation. Journal of Theoretical Biology. 2005 Jul 7; 235(1): 71–83. [PubMed: 15833314]
45. Hohlfeld E, Mahadevan L. Unfolding the Sulcus. Phys Rev Lett. 2011 Mar 7.106(10)
46. Dervaux J, Ben Amar M. Buckling condensation in constrained growth. J Mech Phys Solids. 2011 Mar; 59(3):538–60.
47. Goriely A, Destrade M, Ben Amar M. Instabilities in elastomers and in soft tissues. Q J Mech Appl Math. 2006 Nov.59:615–30.
48. Flügge, W. Viscoelasticity. 2. Berlin; New York: Springer-Verlag; 1975.
49. Kroenke CD, Taber EN, Leigland LA, Knutsen AK, Bayly PV. Regional patterns of cerebral cortical differentiation determined by diffusion tensor MRI. Cereb Cortex. 2009 Dec; 19(12): 2916–29. [PubMed: 19363145]

APPENDIX

A closed-form prediction for cortical wavelength is derived, in terms of the cortical growth rate and the mechanical properties of the cortical and subcortical regions. We follow the analysis by Biot (39) of folding of a viscoelastic plate on a viscoelastic foundation. We begin by modeling the cortex as a thin elastic plate (thickness h, width b, length L, Young's modulus E, Poisson's ratio ν) on a continuous elastic foundation, or core (thickness H, width b, length L, Young's modulus E_f, Poisson's ratio ν_f) undergoing plane strain deformation while under a compressive axial load, P (Fig. A.1). The equation for quasi-static deflections of the plate, neglecting tangential traction forces between the plate and foundation, is:

$$\frac{E}{1-\nu^2}\frac{bh^3}{12}\frac{\partial^4 w}{\partial x^4}+P\frac{\partial^2 w}{\partial x^2}=q \quad \text{A.1}$$

The vertical force per unit length q is related to the deflection w by the stiffness of the foundation. If w is sinusoidal, then q is also sinusoidal with amplitude dependent on the amplitude, w_0, and spatial frequency, γ, of w (39).

$$w = w_0 \cos \gamma x \quad \text{A.2}$$

$$q = q_0 \cos \gamma x \quad \text{A.3}$$

$$q_0 = \frac{-\gamma b E_f}{2(1-\nu_f{}^2)} w_0 \quad \text{A.4}$$

The wavelength of the sinusoidal solution is $\lambda = 2\pi/\gamma$. (As an aside, we note that in the classic Winkler foundation model, represented by an array of linear springs, the foundation stiffness $k = q_0/w_0$ is independent of spatial frequency.) The compressive load, P, on the thin plate can be expressed in terms of the compressive stress, σ_P:

$$P = \sigma_p bh. \quad \text{A.5}$$

Substituting the expressions for w, q, and P above into the equation of equilibrium, and limiting our discussion to the case where both plate and foundation are incompressible ($\frac{E}{1-\nu^2} = 4\mu$ and $\frac{E_f}{1-\nu_f{}^2} = 4\mu_f$) the solution becomes unstable when:

$$\frac{\mu h^3}{3}\gamma^4 - \sigma_p h\gamma^2 = -2\mu_f \gamma, \quad \text{A.6}$$

or

$$\sigma_p = \frac{\mu}{3} h^2 \gamma^2 + \frac{2\mu_f}{h\gamma}. \quad \text{A.7}$$

The critical stress σ_{Pcr} at which a specific harmonic solution becomes unstable depends on the scaled wavenumber $h\gamma = 2\pi h/\lambda$. The solution with minimal critical stress is found by setting $\frac{\partial \sigma_p}{\partial(h\gamma)} = 0$, leading to the following expressions for critical stress and wavelength:

$$\sigma_{Pcr} = 3\mu \left(\frac{\mu}{3\mu_f} \right)^{1/3} \quad \text{A.8}$$

$$\lambda = 2\pi h \left(\frac{\mu}{3\mu_f} \right)^{1/3} \quad \text{A.9}$$

Because stress induces growth over time scale of interest (19) the core does not act like a purely elastic system. Rather it relaxes after the application of stress, like the spring-dashpot foundation in Fig. A.2. This behavior is approximated by the classic Maxwell model of a viscoelastic fluid. For a Maxwell fluid, the force-displacement relation (Eq. A.4) for the foundation is replaced by

$$\dot{q}_0+\frac{1}{\tau_f}q_0=-2\mu_f\gamma b\dot{w}_0 \quad \text{A.10}$$

Defining the operator $R=\frac{d}{dt}$ as in (39), we rewrite the equation above as:

$$q_0=-2\mu_f\gamma b\frac{R}{R+R_f}w_0 \quad \text{A.11}$$

where $R_f=\frac{1}{\tau_f}$ is the rate constant of the foundation. When $R \ll R_f$ the foundation behaves like a fluid; when $R \gg R_f$ it acts like a solid.

Applying the correspondence principle (48), we substitute the new expression into the equation of motion and evaluate the conditions for stability. The critical load and wavelength now depend on R and R_f (39):

$$\sigma_{P_{cr}}=3\mu_f\frac{R}{R+R_f}\left(\frac{\mu(R+R_f)}{3\mu_f R}\right)^{1/3} \quad \text{A.12}$$

$$\lambda=2\pi h\left(\frac{\mu(R+R_f)}{3\mu_f R}\right)^{1/3} \quad \text{A.13}$$

In these expressions it is clear that choosing R to be small (slow deformations) leads to small critical load and long wavelength – the foundation appears soft. When R is large (relatively rapid, but still quasi-static deformation), the critical load increases and the wavelength decreases, approximating the response of a beam on a stiff foundation.

Extension to growth: an elastic layer growing on a viscoelastic foundation

The "viscoelastic rate constant" of the growing foundation is $R_f = 4a\mu_f$ (Eq. 8). To choose the value of the operator R, we consider how long it will take to achieve the critical stress in the growing cortex. If the growth rate in the cortex is G_0, the critical compressive stress $\sigma_{pcr} \approx 4\mu G_0 T_p$, where T_p is the "critical time" when buckling occurs. If we set the value of $R = 1/T_p$, and thus set $\sigma_p = 4\mu G_0/R$ in the equation for the critical stress (A.12) we obtain a polynomial in R.

$$R^5-\frac{64\mu^2{G_0}^3}{9\mu_f^2}(R^2+2R_fR+{R_f}^2)=0 \quad \text{A.14}$$

This equation can be rewritten in terms of the scaled operator $\Gamma = R/R_f$ and the dimensionless parameters $\Gamma_G = G_0/R_f$ and $\beta = \mu/\mu_f$. We obtain:

$$\Gamma^5-\frac{64}{9}\beta^2{\Gamma_G}^3(\Gamma^2+2\Gamma+1)=0 \quad \text{A.15}$$

The existence of at least one positive real root of Eq. A.15 (Eq. 12 in the main text) indicates that the critical load (Eq. A.12) will be reached at the given ratios of growth rate and

material parameters. The corresponding wavelength is given by Eq. A.17 (Eq. 11 in the main text).

$$\frac{\sigma_{Pcr}}{\mu}=\frac{3\Gamma}{\beta(\Gamma+1)}\left(\frac{\beta(\Gamma+1)}{3\Gamma}\right)^{\frac{1}{3}} \quad \text{A.16}$$

$$\frac{\lambda}{h}=2\pi\left(\frac{\beta(\Gamma+1)}{3\Gamma}\right)^{1/3} \quad \text{A.17}$$

Eqs. A.15 – A.17 show that the wavelength and critical stress depend on these two dimensionless parameters: β, the ratio of the short-term elastic moduli of cortex and core, and Γ_G, the ratio of cortical expansion rate to the rate constant of stress-induced growth.

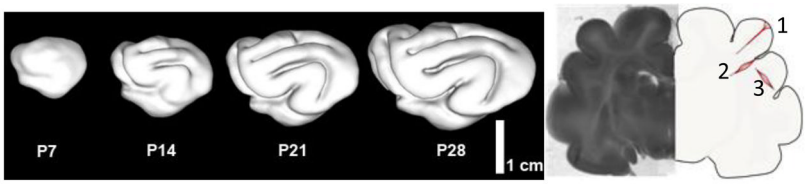

Figure 1.

Summary of cortical folding studies in the ferret (4, 5, 21, 49). (a) Sequence of cortical surfaces generated from longitudinal MR imaging studies in the neonatal ferret. PXX = XX days after birth. (b) Coronal slice of P18 ferret brain near the conclusion of the folding process. The illustration on the right summarizes the results of dissection studies of tissue stress (21). Initial cuts (dotted lines) open when tension is normal to the cut. 1: radial cuts through gyri stay closed (showing lack of tension between gyral walls) except at outer surface, where circumferential tension exists. 2: radial cuts through the bases (fundi) of sulci open in subcortical layers, showing circumferential tension in these locations. 3: circumferential cuts through gyri open, showing radial tension along the axes of gyri.

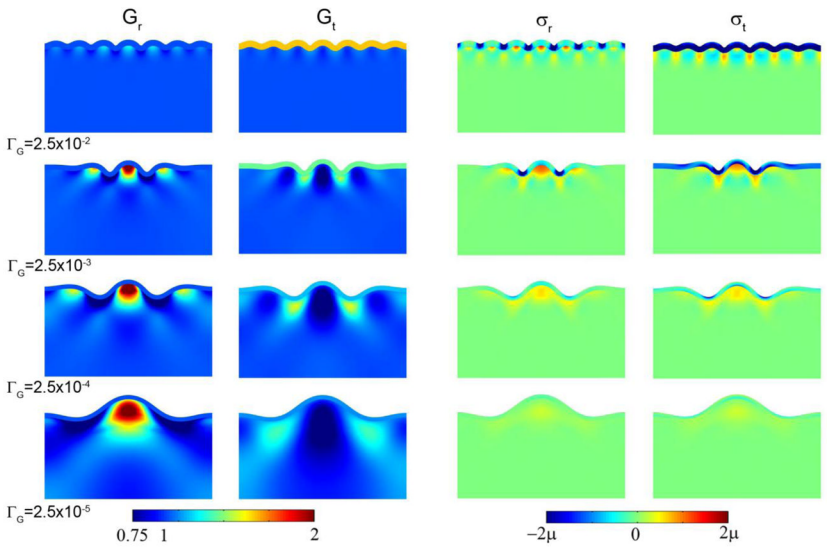

Figure 2.

Effects of cortical growth rate on wavelength, subcortical growth, and stress in the basic model of cortical folding. Target stresses $\bar{\sigma}_{r0} = \bar{\sigma}_{t0} = 0$. Columns: Radial growth G_r; tangential growth G_t; radial stress σ_r; tangential stress σ_t. (Row 1) $\Gamma_G = 2.5\times10^{-2}$, scaled time $\tau = 0.060$; (Row 2) $\Gamma_G = 2.5\times10^{-3}$, $\tau = 0.035$; (Row 3) $\Gamma_G = 2.5\times10^{-4}$, $\tau = 0.014$; (Row 4) $\Gamma_G = 2.5\times10^{-5}$, $\tau = 0.08$. The modulus ratio $\beta = 1$ in all cases.

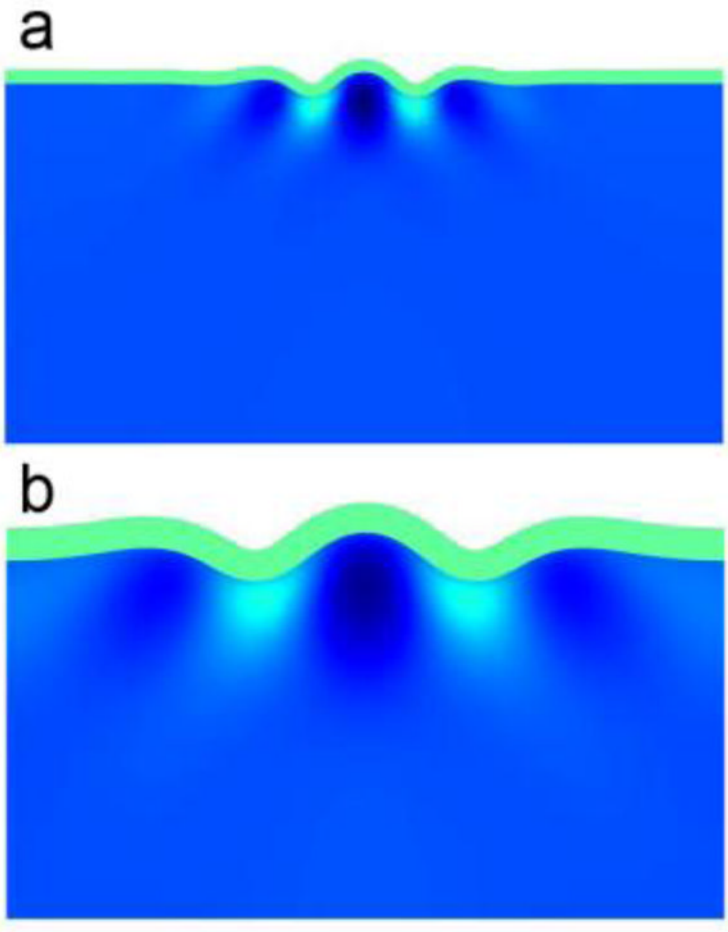

Figure 3.
Folding wavelength is proportional to cortical thickness for a given value of cortical tangential growth rate. (a) Cortical thickness $h = 0.03$. (b) $h = 0.07$. Parameters: $\Gamma_G = 2.5\times10^{-3}$; $\beta = 1$.

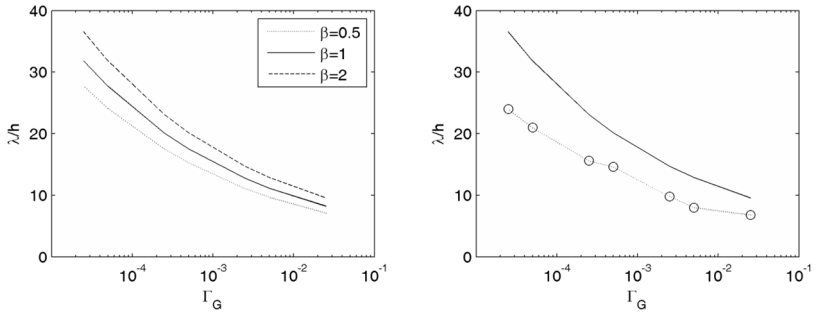

Figure 4.

(a) Effect of cortical growth rate on the gyral wavelength predicted by Eqs. 11–12 for three values of the stiffness ratio β. (b) Solid line: wavelengths predicted from Eqs. 11–12 for β = 1; Dotted line and open circles: wavelengths observed in simulations.

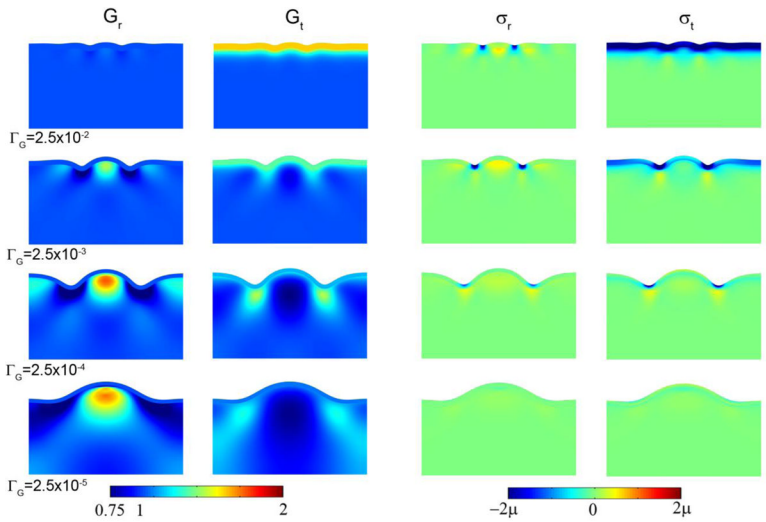

Figure 5.

Effects of cortical growth rate on wavelength, subcortical growth, and stress in the cortical folding model with a compressive target stress in the outer core. Columns: Radial growth G_r; tangential growth G_t; radial stress σ_r; tangential stress σ_t. (Row 1) $\Gamma_G = 2.5\times10^{-2}$, τ, =0.059; (Row 2) $\Gamma_G = 2.5\times10^{-3}$, τ =0.034; (Row 3) $\Gamma_G = 2.5\times10^{-4}$, τ =0.013; (Row 4) $\Gamma_G = 2.5\times10^{-5}$, τ =0.048.

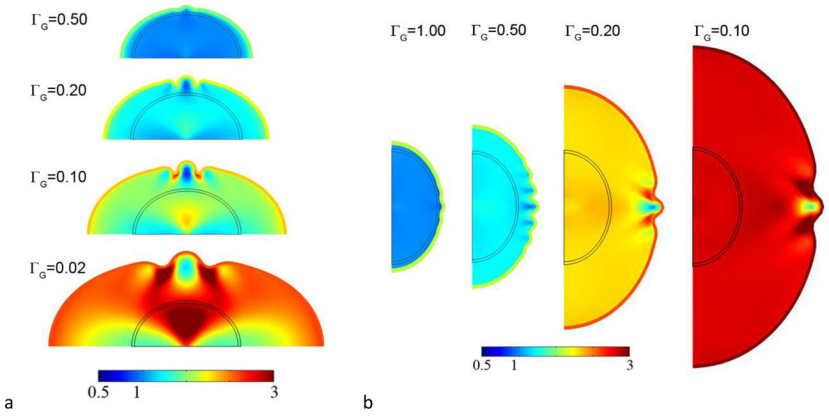

Figure 6.
Folding in (a)the elliptical cylinder (plane strain) model and (b) the axisymmetric ellipsoid model. Color encodes tangential growth G_t.

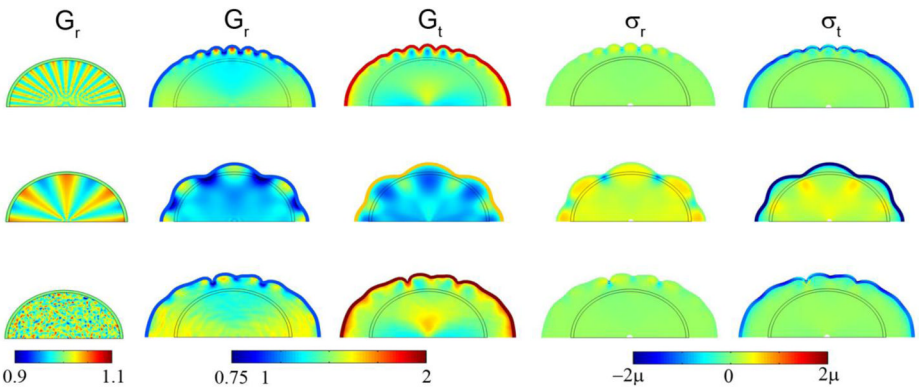

Figure 7.

Effects of initial shape perturbation on wavelength, subcortical growth, and stress in the 2D elliptical (cylinder) model with a compressive target stress in the outer core. Initial radial growth in the core was attained with Eq. 15 with $F(R, \theta, \tau) = F_0 \tau \cos k\theta$ for $\tau < 0.1$. Columns: Initial radial growth G_r at $\tau = 0.10$; radial growth G_r; tangential growth G_t; radial stress σ_r; tangential stress σ_t. Row 1: $F(r, \theta, \tau) = 10\tau \cos 32\theta$ for $\tau < 0.10$, shown at $\tau = 0.90$. Row 2: $F(r, \theta, \tau) = 10\tau \cos 8\theta$ for $\tau < 0.10$, shown at $\tau = 0.60$; Row 3: $F(r, \theta, \tau) = 50\tau$ random (r, θ) for $\tau < 0.1$, shown at $\tau = 1.2$. In all rows $\Gamma_G = 0.20$.

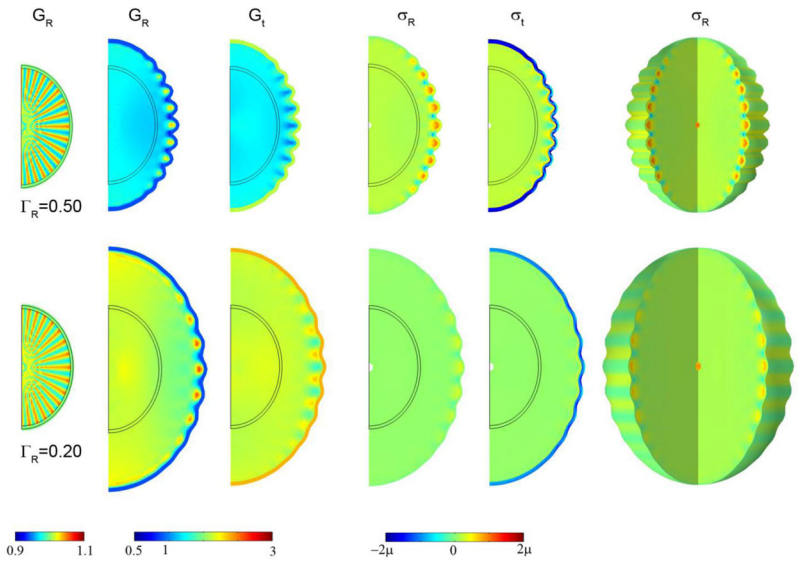

Figure 8.

Effects of cortical growth on wavelength, subcortical growth, and stress in the axisymmetric ellipsoid model. Initial radial growth in the core was attained with Eq. 15 with $F(R, \theta, \tau) = 10\tau \cos 32\theta$ for $\tau < 0.1$. Columns: Initial radial growth G_R at $\tau = 0.10$; radial growth G_R; tangential growth G_t; radial stress σ_r; tangential stress σ_t; 3D view of radial stress σ_r. Row 1: $\Gamma_G = 0.50$, $\tau = 0.90$; Row 2: $\Gamma_G = 0.20$, $\tau = 1.25$.

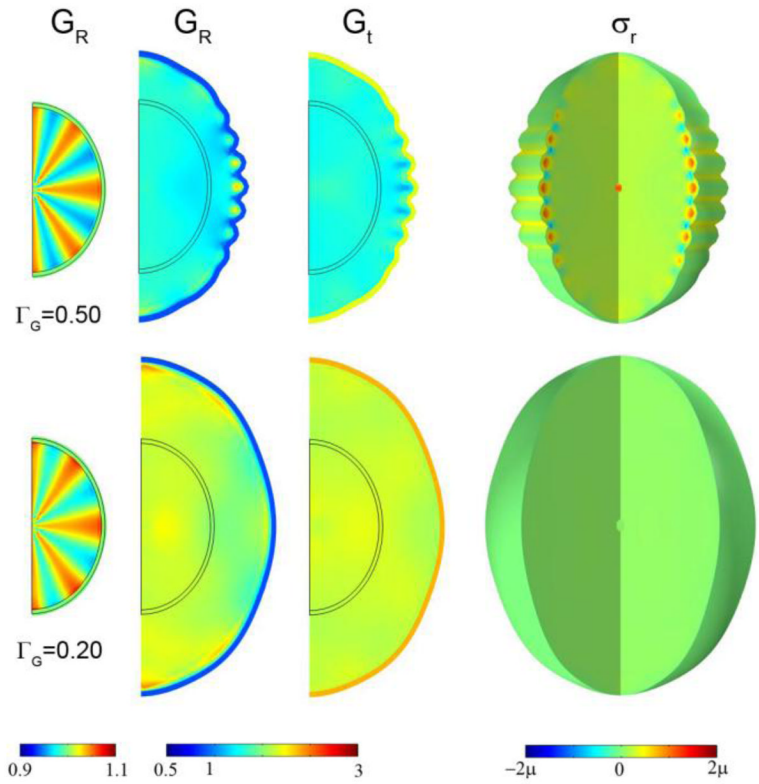

Figure 9.

The effects of cortical growth rate and small variations in initial conditions. Initial radial growth in the core was imposed according to Eq. 15 with $F(R, \theta, \tau) = 10\tau \cos 8\theta$ for $\tau <$ 0.10. Columns: Initial radial growth G_R at τ =0.10; radial growth G_R; tangential growth G_t; 3D view of radial stress σ_r. Row 1: Γ_G = 0.50, τ =0.90; Row 2: Γ_G = 0.20, τ =1.25.

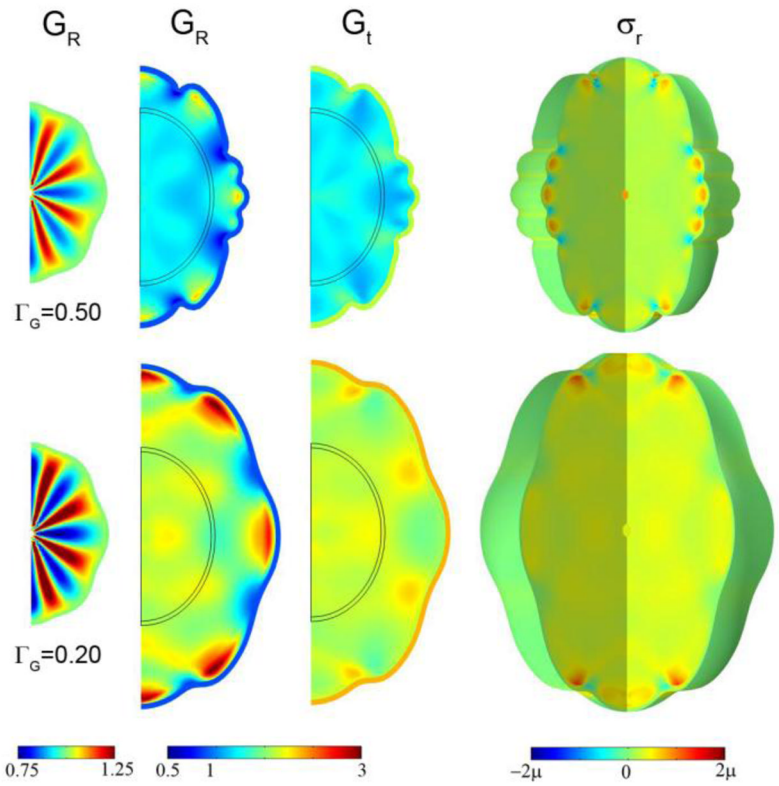

Figure 10.

The effects of cortical growth rate and larger initial perturbations. Initial radial growth in the core was imposed according to Eq. 15 with $F(R, \theta, \tau) = 50\tau \cos 8\theta$ for $\tau < 0.10$. Columns: Initial radial growth G_R at $\tau = 0.10$; radial growth G_R; tangential growth G_t; 3D view of radial stress σ_r. Row 1: $\Gamma_G = 0.50$, $\tau = 0.90$; Row 2: $\Gamma_G = 0.20$, $\tau = 1.25$.

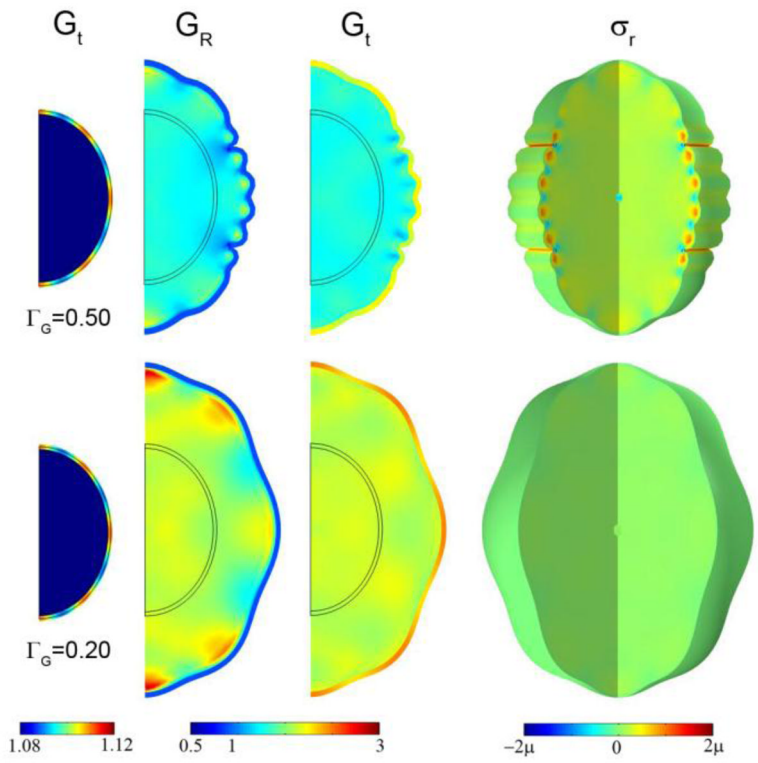

Figure 11.

The effect of spatial variation of cortical growth rate. Spatial variations of tangential growth in the cortex were imposed according to Eq. 16 with $G_t = 1 + \tau(1 + 0.1 \cos 8\theta)$. Columns: Tangential growth G_t at τ =0.10; radial growth G_R; tangential growth G_t; 3D view of radial stress σ_r. Row 1: $\Gamma_G = 0.50$, τ =1.00; Row 2: $\Gamma_G = 0.20$, τ =1.25.

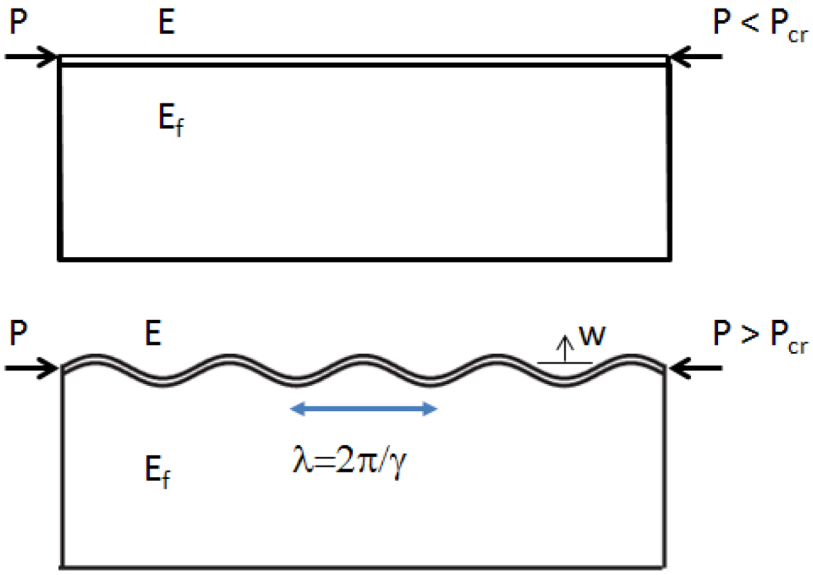

Figure A.1.
A thin elastic beam on an elastic foundation, under compressive loading.

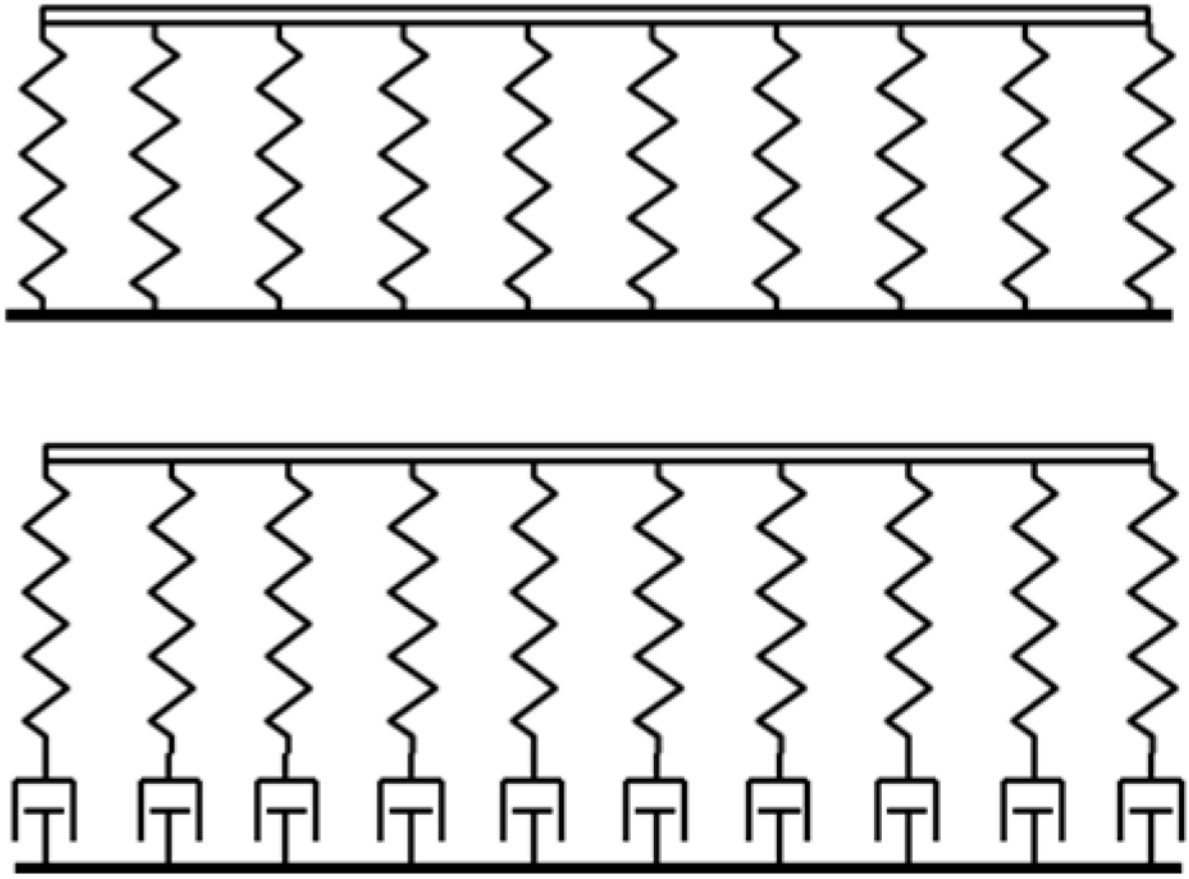

Figure A.2.
(a) If no subcortical growth occurs in response to stress, the cortex is like the beam on an elastic foundation. (b) If growth occurs in response to stress, the core acts like a viscoelastic (Maxwell) foundation, responding like a solid for fast deformations and like a fluid at slow strain rates.